VNU Journal of Science: Mathematics – Physics, Vol. 39, No. 3 (2023) 106-115

VNU Journal of Science: Mathematics - Physics

Journal homepage: https://js.vnu.edu.vn/MaP

Original Article

Characterization of Fe_2O_3 Nanopowder Synthesized by Sol-Gel Method for Energy Storage Applications

Bui Thi Hang*

International Training Institute for Materials Science, Hanoi University of Science and Technology, 1 Dai Co Viet, Hanoi, Vietnam

Received 26 April 2023
Revised 17 May 2023; Accepted 26 May 2023

Abstract: Fe_2O_3 nanopowder was synthesized by sol-gel method from the iron source material $Fe(NO_3)_3.9H_2O$ and citric acid $C_6H_8O_7.H_2O$ without any refined process. The structure and particles size of the synthesized materials were determined by X-ray diffraction and scanning electron microscopy. The obtained product is α-Fe_2O_3 with different shapes and sizes depending on the preparation conditions. α-Fe_2O_3 was applied as anode of iron-air battery. The cyclic voltammetry measurements showed that the size and morphology of Fe_2O_3 particles affect the electrochemical characteristics of the electrodes. Using K_2S as an electrolyte additive improved the electrochemical properties of mixing of Fe_2O_3 and carbon acetylene black (Fe_2O_3/AB) electrodes as evidenced by increased redox reaction rate of iron, increased capacity of Fe_2O_3/AB electrode and reduced H_2 evolution.

Keywords: Fe_2O_3 nanopowders, Fe_2O_3 nanoparticles, sol-gel, Fe_2O_3/AB electrode, energy storage.

1. Introduction

Rechargeable iron/air batteries have been attracting the attention of many researchers due to their high theoretical specific capacity (960 mAh/g), long cycle life, low cost and environmental friendliness [1-10]. Fe/air batteries can be used as a power supply for electric vehicles and hybrid electric vehicles. However, the practical applications of iron/air batteries are limited by the thermodynamic instability of iron in alkaline solution [11], the low discharge rate, high self-discharge, the hydrogen evolution reaction occurs simultaneously with the iron reduction reaction during the charging process, leading to

* Corresponding author.
E-mail address: hang@itims.edu.vn/hang.buithi@hust.edu.vn

https//doi.org/10.25073/2588-1124/vnumap.4878

low discharge-charge efficiency of the battery [12-14]. In addition, the passivation caused by iron (II) hydroxide formed during the discharge prevents the oxidation reaction of the inner iron layer of the electrode.

To solve above mentioned problems of iron/air batteries, some additives for electrodes and electrolyte solutions have been used [6-11, 15-18]. Some researchers used conduction additives such as acetylene black to improve the conductivity of electrode, whereas others used sulfide additives to increases the anodic dissolution of iron metal and avoid the electrode passivation. There are also researchers who used both the carbon and sulfide additives: Sulfides suppressed the hydrogen evolution, accelerate the redox reaction of iron, helped the iron electrode to maintain high discharge current. Acetylene black helped to electrically connect up the insulating discharged product and therefore more active material can participate in the electrode reaction.

In iron/air batteries, the iron electrode plays an important role, deciding the capacity and performance of the battery. Finding a method to produce iron oxides with a low cost and a good quality is an important step to reduce the product price and improve the efficiency of iron/air batteries. Therefore, the objective of this work is to prepare Fe_2O_3 nanoparticles by sol-gel method and to identify the parameters controlling the particles size [19]. This is a simple and inexpensive method that can be used to produce large amounts of iron oxide per fabrication. The Fe_2O_3 powder synthesized by this method is expected to mitigate the existing limitations of iron electrodes and reducing production costs for iron/air batteries.

2. Experimental

2.1. Preparation of Fe_2O_3 Nanoparticles

Iron nitrate $Fe(NO_3)_3.9H_2O$ (Aldrich 98%) was used as iron source and monohydrated citric acid $C_6H_8O_7.H_2O$ (Aldrich 99%) as ligand molecules and distilled water as the solvent. All chemicals were used without further purification. 100 ml of iron nitrate solution was dropped into 100 ml citric acid solution with vigorous stirring. The obtained solution was then heated to 70 °C while maintaining vigorous stirring until the contained water was evaporated and the gel was formed. The dried gel was annealed at 400 °C to get Fe_2O_3 nanoparticles. The concentration of iron nitrate was kept at 0.1 M whereas citric acid concentration was changed from 0.05 M to 0.5 M to control the shape and size of iron oxide particles. The volume of citric acid was also increased to 800 ml at the concentration of 0.2 M to vary the product size. The preparation conditions of various samples were shown in the Table 1.

Table 1. Samples and their preparation conditions by sol-gel method

No	Sample name of Fe_2O_3	Preparation conditions
1	100 ml-0.05 M	100 ml $Fe(NO_3)_3$ 0.1 M + 100 ml $C_6H_8O_7$ 0.05 M, T=400 °C
2	100 ml-0.2 M	100 ml $Fe(NO_3)_3$ 0.1 M + 100 ml $C_6H_8O_7$ 0.2 M, T=400 °C
3	100 ml-0.5 M	100 ml $Fe(NO_3)_3$ 0.1 M + 100 ml $C_6H_8O_7$ 0.5 M, T=400 °C
4	800 ml-0.2 M	100 ml $Fe(NO_3)_3$ 0.1 M + 800 ml $C_6H_8O_7$ 0.2 M, T=400 °C

2.2. Characterisation

The crystalline structure of synthesized α-Fe_2O_3 nanopowder was characterized by X-ray diffraction (XRD; Rigaku), using CuK_α radiation ($\lambda_{K\alpha}$ = 0.15406 nm, U = 40 kV, I = 150 mA) and 2θ range of 20 to 80°. The particles size and morphologies of the as-prepared materials were examined by a Field-Emission scanning electron microscopy (FE-SEM, Hitachi-4800).

To determine the electrochemical behavior of synthesized α-Fe_2O_3 materials, the electrode sheet was fabricated by mixing 45 wt.% of the respective Fe_2O_3, 45 wt.% of the carbon acetylene black (AB) as additive and 10 wt.% polytetrafluoroethylene (PTFE; Daikin Co.) as binder, and then rolling. The Fe_2O_3/AB electrodes were punched from electrode sheets into pellets of 1 cm diameter and then pressed onto the Titanium mesh with a pressure of about 150 kg cm^{-2}.

Cyclic voltammetry (CV) measurements were performed using a three-electrode glass cell with Fe_2O_3/AB as the working electrode (WE), Pt mesh as the counter electrode (CE) and Hg/HgO as the reference electrode (RE). The electrolyte was 8 mol dm^{-3} aqueous KOH solution. The effect of electrolyte additive K_2S was investigated using electrolyte containing 7.99 M KOH and 0.01 M K_2S aqueous solution. The CV measurements were taken at a scan rate of 5 mV s^{-1} and within a range of –1.3 V to –0.1 V.

3. Results and Discussion

3.1. Crystal Structure and Morphology of Synthesized Materials

The X-ray patterns of the synthesized Fe_2O_3 powder are presented in Fig. 1. In all cases from 0.05 M to 0.50 M citric acid, XRD patterns exhibit characteristic diffraction peaks at 2θ values of 24.13°; 33.11°; 35.61°; 40.83°; 49.41°; 53.99°; 57.49°; 62,38° and 63.96° corresponding to (012), (104), (110), (113), (024), (116), (018), (214) and (300) crystalline planes, respectively. These diffraction peaks match with patterns of the α-Fe_2O_3 phase reported in ICSD No.033-0664. No other reflections are detected in the XRD patterns, thereby one can suggest that the synthesized products are pure α-Fe_2O_3. Therefore, α-Fe_2O_3 powder was successfully prepared by the sol-gel method.

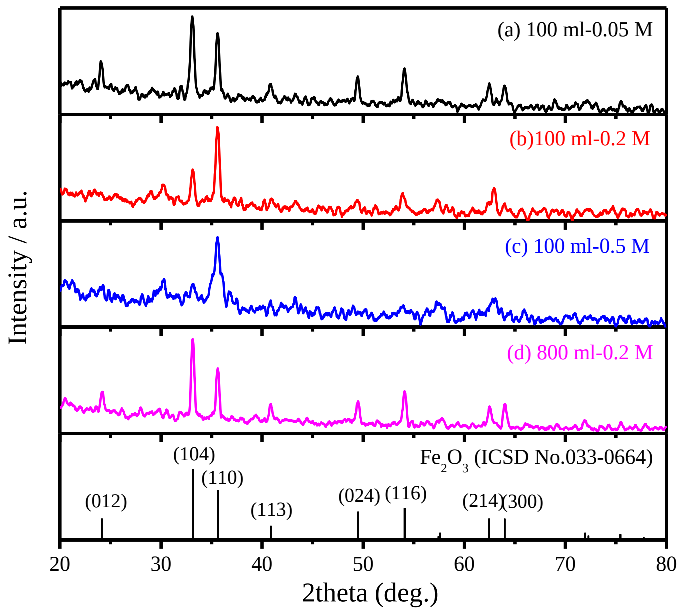

Figure 1. X-ray patterns of the synthesized α-Fe_2O_3 with (a) 100 ml-0.05 M, (b) 100 ml-0.2 M, (c) 100 ml-0.5 M and (d) 800 ml-0.2 M citric acid.

FE-SEM was used to investigate the particles size and surface morphology of α-Fe_2O_3, the obtained results are shown in Fig. 2. The effects of citric acid concentration on the size and shape of α-Fe_2O_3 particles under the same experimental conditions were clearly shown in Fig. 2. Using low citric acid concentration, i.e. 0.05 M, α-Fe_2O_3 look like polyhedral particles (Fig. 2a). Increasing citric acid to 0.2 M and 0.5 M, a cubic (Fig. 2b) and spherical shape (Fig. 2c) of α-Fe_2O_3 were formed, respectively. Keep the concentration of citric acid at 0.2 M and increasing amount from 100 ml to 800 ml, the aggregation of Fe_2O_3 nanoparticles occurred resulting in larger Fe_2O_3 particles (Fig. 2d). Fe_2O_3 particles with different sizes and shapes will have different effects on the electrochemical properties of the Fe_2O_3 electrode. By changing the synthesis conditions during the sol-gel process, one can control the shape and size of the Fe_2O_3 particles to achieve the desired particle size and shape.

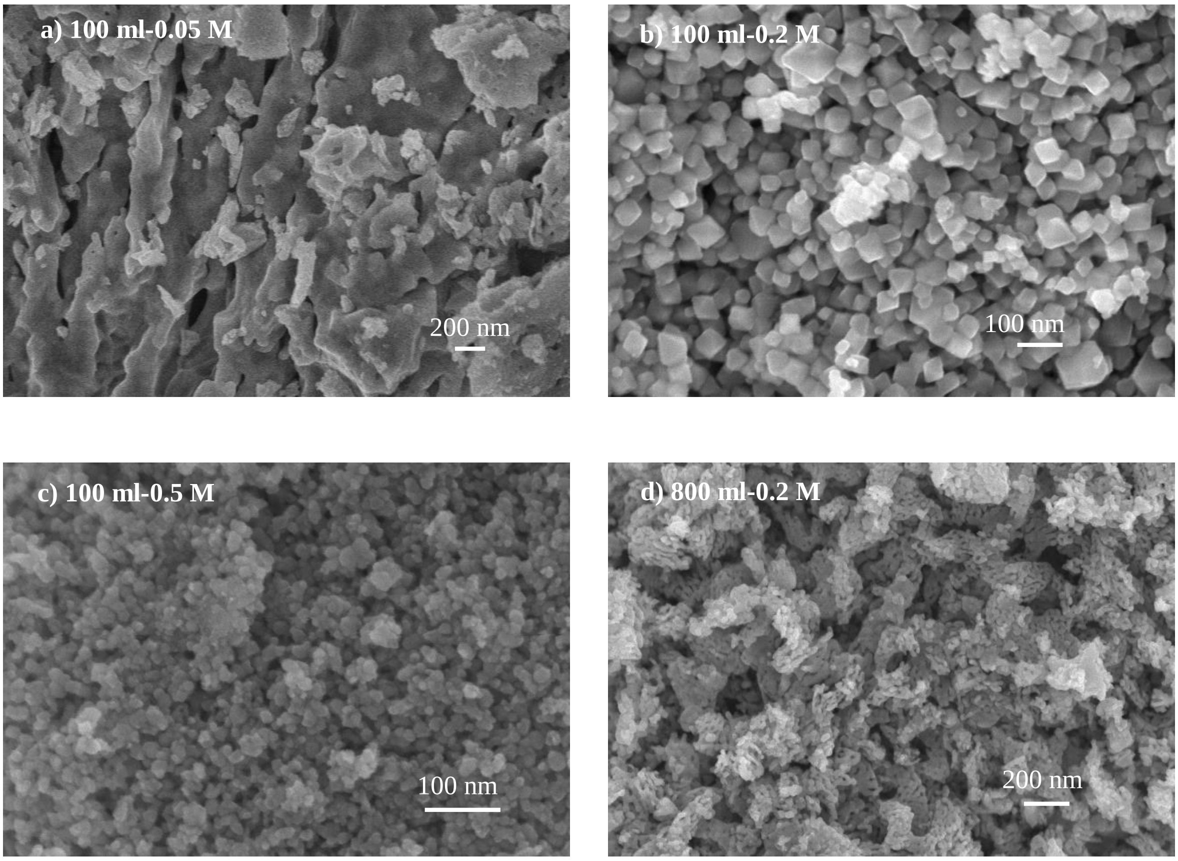

Figure 2. FE-SEM images of the synthesized α-Fe_2O_3 with (a) 100 ml-0.05 M, (b) 100 ml-0.2 M, (c) 100 ml-0.5 M and (d) 800 ml-0.2 M citric acid.

3.2. Electrochemical Characterization

The CV profiles of the Fe_2O_2/AB electrodes using Fe_2O_3 synthesized by sol-gel method as active material and AB as carbon additive are shown in Fig. 3. When scanning from −1.3 V to −0.1 V, three oxidation peaks appear at about −1.0 V (a_0), −0.75 V (a_1), −0.6 V (a_2) and two reduction peaks appears at about −1.1 V (c_2) and −1.2 V (c_1) in reverse scan but c_1 reduction peak is almost overlapped by H_2 evolution peak. The small a_0 peak is due to the OH^- group adsorption of the iron electrode to form

[$Fe(OH)_{ad}$] before being oxidized to $Fe(OH)_2$. The anodic peak (a_1) is attributed to the oxidation of Fe to $Fe(OH)_2$ and anodic peak (a_2) is attributed to the oxidation of $Fe(OH)_2$ to Fe(III). Thus, the anodic peak a_1 and cathodic peak c_1 correspond to the Fe/Fe(II) redox couple (Eq. 1), and the anodic peak (a_2) and the cathodic peak (c_2) correspond to the Fe(II)/Fe(III) redox couple (Eqs. 2 and/or 3).

$Fe + 2OH^- \rightleftharpoons Fe(OH)_2 + 2e$ (1) ($E^0 = -0.975$ V vs. Hg/HgO) [20]

$Fe(OH)_2 + OH^- \rightleftharpoons FeOOH + H_2O + e$ (2) ($E^0 = -0.658$ V vs. Hg/HgO) [20]

and/or $3Fe(OH)_2 + 2OH^- \rightleftharpoons Fe_3O_4.4H_2O + 2e$ (3) ($E^0 = -0.758$ V vs. Hg/HgO) [21]

The cathodic peak corresponding to reduction of $Fe(OH)_2$ to Fe (c_2) is not visible, probably because it was superimposed on the current for the hydrogen evolution reaction. The hydrogen evolution reaction competes with the electrode charge reaction and results in low cycling efficiency of Fe_2O_3 electrode.

The oxidation peaks shifted towards the negative potential while the reduction peaks moved to the more positive side when repeated cycling, indicating that the overpotential of the redox reaction of iron reduced. This behavior will give positive effects on the cycling of the iron electrode. However, the redox current reduced with the increased number of cycles.

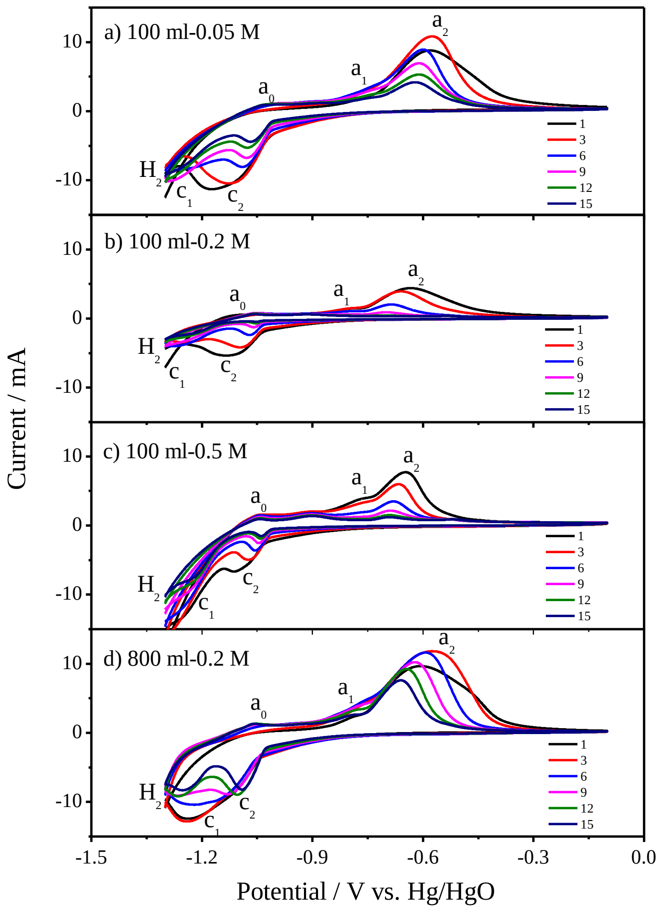

Figure 3. CV profiles of Fe_2O_3/AB composite electrodes with Fe_2O_3:AB:PTFE = 45:45:10 wt.% in KOH solution with Fe_2O_3 synthesized at (a) 100 ml-0.05 M, (b) 100 ml-0.2 M, (c) 100 ml-0.5 M and (d) 800 ml-0.2 M citric acid.

Comparing the CV profiles of all the samples each other shows that the Fe_2O_3 samples synthesized at citric acid concentration of 100 ml-0.05 M (Fig. 3a) and 800 ml-0.2 M (Fig. 3d) give higher a_2/c_2 redox couple peak than the other samples, demonstrating that they have better cyclability than others. FE-SEM images of the samples in Fig. 2 show that at the citric acid concentration of 100 ml-0.2 M (Fig. 2b) and 100 ml-0.5 M (Fig. 2c) Fe_2O_3 particles have relatively uniform cubic and spherical shape, respectively, but the sample of 100 ml-0.05 M (Fig. 2a) and 800 ml-0.2 M (Fig. 2d) have polyhedral shape and larger particle size. This result proved that the shape and size of the Fe_2O_3 particles have a strong effect on their cyclability. Due to the agglomeration of small Fe_2O_3 to form larger particles, the internal resistance of these samples is smaller than that of samples which have smaller Fe_2O_3 leading to their higher redox current.

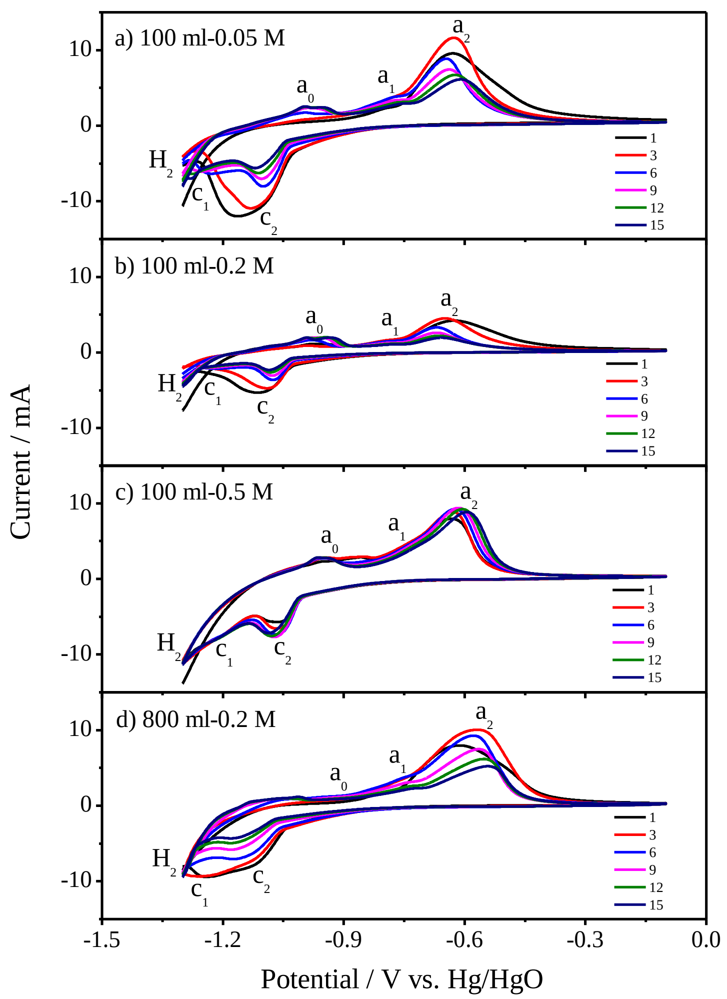

Figure 4. CV profiles of Fe_2O_3/AB composite electrodes with Fe_2O_3:AB:PTFE = 45:45:10 wt.% in KOH+K_2S solution with Fe_2O_3 synthesized at (a) 100 ml-0.05 M, (b) 100 ml-0.2 M, (c) 100 ml-0.5 M and (d) 800 ml-0.2 M citric acid.

To investigate the influence of K_2S additive on the electrochemical properties of the iron electrode, the CV measurement of Fe_2O_3/AB electrode with Fe_2O_3:AB:PTFE = 45:45:10 (%) was carried-out in the electrolyte solution of 7.99 M KOH + 0.01 M K_2S, the results are shown in Fig. 4. With the presence of K_2S in the electrolyte solution, the sharp redox peaks appeared at the same potential range as Fe_2O_3/AB electrodes in KOH (Fig. 3). However, the oxidation peak a_0 was higher and especially the redox current under the Fe(II)/Fe(III)(a_2/c_2) couple peaks decreased more slowly with the cycling number. For the 100 ml-0.5 M citric acid sample (Fig. 4c), its redox current intensity was maintained when repeating 15 cycles. This result demonstrated the positive effect of K_2S additive on the redox reaction of iron. It may be due to the S^{2-} ion combines into the iron oxide and interacts with Fe(I), Fe(II) or Fe(III) in the oxide film to stimulate the decomposition of iron [22, 23] and increase the electric conductivity of the electrode [8, 13] thereby improving the cyclability of iron.

To evaluate the role of K_2S additive in the electrolyte solution for Fe_2O_3/AB electrode, the discharge capacity was calculated from the CV results of Fe_2O_3/AB electrodes in KOH (Fig. 3) and KOH + K_2S (Fig. 4), the results are shown in Fig. 5. Discharge capacities of all electrodes in KOH electrolyte solution (Fig. 5a) are lower than those in electrolyte solution containing K_2S (Fig. 5b) and rapidly decreased with repeated cycling. This confirmed that the presence of K_2S in the electrolyte increased the discharge capacity and improved the cyclability of the iron electrode.

Comparing the discharge capacities of samples prepared by sol-gel method in an electrolyte solution containing K_2S (Fig. 5b) each other, one can see that the 100ml-0.5M citric acid sample has a relatively stable specific capacity while the other samples have gradually decreased specific capacity with the number of cycles. SEM image of 100 ml-0.5 M citric acid sample (Fig. 2c) showed that Fe_2O_3 has spherical shape and their particles size is the smallest. This proves that the size and morphology of Fe_2O_3 particles have significant influence on their cyclability. Thus, among the Fe_2O_3 materials synthesized by sol-gel method, the sample produced at 100 ml-0.5 M citric acid gave the largest discharge capacity, thereby it is the most suitable material for iron-air batteries.

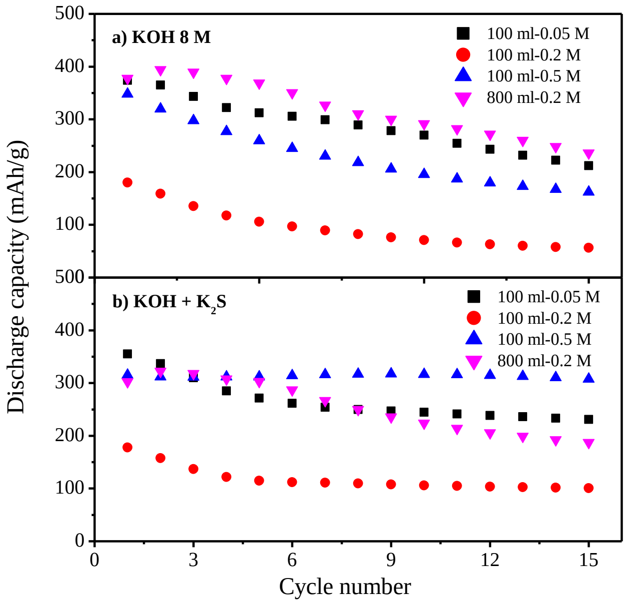

Figure 5. The variation of discharge capacity with the number of cycles of the Fe_2O_3/AB electrode in (a) KOH and (b) KOH + K_2S solutions.

One of the important roles of the K_2S additive in the electrolyte solution is to reduce the amount of H_2 generated during the charging process, leading to improve the efficiency, capacity, and energy of the electrode. To clarify this hypothesis, the amount of H_2 evolution was calculated from the CV measurement in KOH (Fig. 3) and KOH + K_2S (Fig. 4) and the results are shown in Fig. 6. The currents come from H_2 evolution at the electrodes in the electrolyte solution containing K_2S (Fig. 6b) are smaller than those in the electrolyte solution without K_2S additive (Fig. 6a). This demonstrates that in the presence of K_2S in the electrolyte solution, the amount of H_2 evolution has been reduced during the reaction. This is positive effect of K_2S on the capacity, as well as the discharge - charge efficiency of the Fe_2O_3/AB electrode.

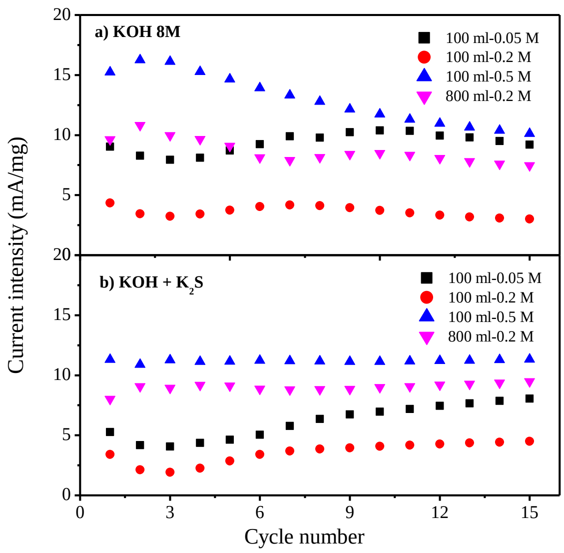

Figure 6. The variation of hydrogen evolution with the number of cycles of the Fe_2O_3/C electrodes in (a) KOH and (b) KOH + K_2S solutions.

4. Conclusion

Nanaostructured Fe_2O_3 powder materials with different particles sizes and shapes have been successfully synthesized by sol-gel method. Investigation of the electrochemical properties shows that the size and morphology of Fe_2O_3 particles strongly affect their cyclability. The size and morphology of Fe_2O_3 particles can be controlled by changing the concentration of precursors during sol-gel process to give the best electrochemical characteristics. The positive effect of K_2S additive on the electrochemical properties of Fe_2O_3/AB electrode is confirmed by the increase in both the redox reaction rate of iron and the capacity of Fe_2O_3/AB electrode, simutaneously the reduce of H_2 evolution. From the obtained results one can suggest that nanostructured Fe_2O_3 materials synthesized by sol-gel method can be a potential candidate for iron-air battery anode.

Acknowledgment

This research is funded by the Ministry of Education and Training (MOET) under grant number B2022-BKA-13. The author would like to thank.

References

[1] A. Ito, L. Zhao, S. Okada, J. Yamaki, Synthesis of Nano-Fe3O4-loaded Tubular Carbon Nanofibers and Their Application as Negative Electrodes for Fe/air Batteries, J. Power Sources, Vol. 196, No. 19, 2011, pp. 8154-8159, https://doi.org/10.1016/j.jpowsour.2011.05.043.

[2] A. Inoishi, T. Sakai, Y.W. Ju, S. Ida, T. Ishihara, Improved Cycle Stability of Fe–Air Solid State Oxide Rechargeable Battery Using Lagao3-Based Oxide Ion Conductor, J. Power Sources, Vol. 262, 2014, pp. 310-315, https://doi.org/10.1016/j.jpowsour.2014.03.125.

[3] A. K. Manohar, C. Yang, S. R. Narayanan, The Role of Sulfide Additives in Achieving Long Cycle Life Rechargeable Iron Electrodes in Alkaline Batteries, J. Electrochem. Soc., Vol. 162, No. 9, 2015, pp. A1864-A1872, https://doi.org/10.1149/2.0741509jes.

[4] H. A. F. Rodríguez, R. D. M. Kerracher, C. P. D. León, F. C. Walsh, Improvement of Negative Electrodes for Iron-Air Batteries: Comparison of Different Iron Compounds as Active Materials, J. Electrochem. Soc., Vol. 166, No. 2, 2019, pp. A107-A117, https://doi.org/10.1149/2.1071816jes.

[5] H. A. F. Rodríguez, R. D. M. Kerracher, M. Insausti, A. G. Luis, C. P. D. León, C. Alegre, V. Baglio, A. S. Aricò, F. C. Walsh, A Rechargeable, Aqueous Iron Air Battery with Nanostructured Electrodes Capable of High Energy Density Operation, J. Electrochem. Soc, Vol. 164, No. 6, 2017, pp. A1148-A1157, https://doi.org/10.1149/2.0711706jes.

[6] A. S. Rajan, S. Sampath, A. K. Shukla, An in Situ Carbon-grafted Alkaline Iron Electrode for Iron-Based accumulators, Energy Environ. Sci., Vol. 7, No. 3, 2014, pp. 1110-1116, https://doi.org/10.1039/c3ee42783h.

[7] J. O. Gil Posada, P. J. Hall, Post-hoc Comparisons Among Iron Electrode Formulations Based on Bismuth, Bismuth Sulphide, Iron Sulphide, and Potassium Sulphide Under Strong Alkaline Conditions, J. Power Sources, Vol. 268, 2014, pp. 810-815, https://doi.org/10.1016/j.jpowsour.2014.06.126.

[8] X. Zhang, X. G. Wang, Z. Xie, Z. Zhou, Recent Progress in Rechargeable Alkali Metal–air Batteries, Green Energy Environ, Vol. 1, No. 1, 2016, pp. 4-17, https://doi.org/10.1016/j.gee.2016.04.004.

[9] Q. Fang, C. M. Berger, N. H. Menzler, M. Bram, L. Blum, Electrochemical Characterization of Fe-air Rechargeable Oxide Battery in Planar Solid Oxide Cell Stacks, J. Power Sources, Vol. 336, 2016, pp. 91-98, https://doi.org/10.1016/j.jpowsour.2016.10.059.

[10] K. Hayashi, Y. Wada, Y. Maeda, T. Suzuki, H. Sakamoto, W. K. Tan, G. Kawamura, H. Muto, A. Matsuda, Electrochemical Performance of Sintered Porous Negative Electrodes Fabricated with Atomized Powders for Iron-Based Alkaline Rechargeable Batteries, J. Electrochem. Soc, Vol. 164, No. 9, 2017, pp. A2049-A2055, https://doi.org/10.1149/2.1311709jes.

[11] T. S. Balasubramanian, A. K. Shukla, Effect of Metal-sulfide Additives on Charge/Discharge Reactions of the Alkaline Iron Electrode, J. Power Sources, Vol. 41, No. 1-2, 1993, pp. 99-105, https://doi.org/10.1016/0378-7753(93)85008-C.

[12] J. O. G. Posada, P. J. Hall, Controlling Hydrogen Evolution on Iron Electrodes, Int. J. Hydrogen Energy., Vol. 41, No. 45, 2016, pp 20807-20817, https://doi.org/10.1016/j.ijhydene.2016.04.123.

[13] C. A. C. Souza, I. A. Carlos, M. Lopes, G. A. Finazzi, M. R. H. D. Almeida, Self-discharge of Fe-Ni alkaline Batteries, J. Power Sources, Vol. 132, No. 1-2, 2004, pp. 288-290, https://doi.org/10.1016/j.jpowsour.2003.12.043.

[14] C. Yang, A. K. Manohar, S. R. Narayanan, A High-Performance Sintered Iron Electrode for Rechargeable Alkaline Batteries to Enable Large-Scale Energy Storage, J. Electrochem. Soc., Vol. 164, No. 2, 2017, pp. A418-A429, https://doi.org/10.1149/2.1161702jes.

[15] M. K. Ravikumar, A. S. Rajan, S. Sampath, K. R. Priolkar, A. K. Shukla, In Situ Crystallographic Probing on Ameliorating Effect of Sulfide Additives and Carbon Grafting in Iron Electrodes, J. Electrochem. Soc., Vol. 162, No. 12, 2015, pp. A2339-A2350, https://doi.org/10.1149/2.0721512jes.

[16] B. T. Hang, S. H. Yoon, S. Okada, J. Yamaki, Effect of Metal-Sulfide Additives on Electrochemical Properties of Nano-sized Fe2O3-loaded Carbon for Fe/Air Battery Anodes, J. Power Sources, Vol. 168, No. 2, 2007, pp. 522-532, https://doi.org/10.1016/j.jpowsour.2007.02.067.

[17] A. Sundar Rajan, M. K. Ravikumar, K. R. Priolkar, S. Sampath, A. K. Shukla, Carbonyl-Iron Electrodes for Rechargeable-Iron, Electrochem. Energy Technol., Vol. 1, 2014, pp. 2-9, https://doi.org/10.1515/eetech-2014-0002.

[18] D. Mitra, A. S. Rajan, A. Irshad, S. R. Narayanan, High Performance Iron Electrodes with Metal Sulfide Additives, J. Electrochem. Soc., Vol. 168, No. 3, 2021, pp. 030518, https://doi.org/10.1149/1945-7111/abe9c7.

[19] M. M. B. Abbad, M. S. Takriff, A. Benamor, A. W. Mohammad, Size and Shape Controlled of α-Fe2O3 Nanoparticles Prepared Via Sol–gel Technique and Their Photocatalytic Activity, J. Sol-Gel Sci. Technol., Vol. 81, No. 3, 2017, pp. 880-893, https://doi.org/10.1007/s10971-016-4228-4.

[20] C. Chakkaravarthy, P. Periasamy, S. Jegannathan, K. I. Vasu, The Nickel/Iron Battery, J. Power Sources, Vol. 35, No. 1, 1991, pp. 21-35, https://doi.org/10.1016/0378-7753(91)80002-F.

[21] K. Micka, Z. Zábranský, Study of Iron Oxide Electrodes in an Alkaline Electrolyte, J. Power Sources, Vol. 19, No. 4, 1987, pp. 315-323, https://doi.org/10.1016/0378-7753(87)87007-6.

[22] L. Öjefors, SEM Studies of Discharge Products from Alkaline Iron Electrodes, J. Electrochem. Soc., Vol. 123, No. 11, 1976, pp. 1691-1696, https://doi.org/10.1149/1.2132669.

[23] M. C. Wu, T. S. Zhao, P. Tan, H. R. Jiang, X. B. Zhu, Cost-effective carbon Supported Fe_2O_3 Nanoparticles as an Efficient Catalyst for Non-Aqueous Lithium-Oxygen Batteries, Electrochim. Acta., Vol. 211, 2016, pp. 545-551, https://doi.org/10.1016/j.electacta.2016.05.147.